Hybridization of quantum plasmon modes in coupled nanowires: From the classical to the tunneling regime

Kirsten Andersen,[*] Kristian L. Jensen, and Kristian S. Thygesen

Center for Atomic-scale Materials Design, Department of Physics

Technical University of Denmark, DK - 2800 Kgs. Lyngby, Denmark

(Dated: April 18, 2013)

Abstract

We present full quantum mechanical calculations of the hybridized plasmon modes of two nanowires at small separation, providing real space visualization of the modes in the transition from the classical to the quantum tunneling regime. The plasmon modes are obtained as certain eigenfunctions of the dynamical dielectric function which is computed using time dependent density functional theory (TDDFT). For freestanding wires, the energy of both surface and bulk plasmon modes deviate from the classical result for low wire radii and high momentum transfer due to effects of electron spill-out, non-local response, and coupling to single-particle transitions. For the wire dimer at separations 1.5-0.3 nm, the spatial shape and energy of the plasmon modes are continuously altered with distance and deviate from the classical result due to the increasing overlap of unoccupied electronic states of the two wires (virtual tunneling). At separations around 2-3 Å electrons at the Fermi energy can tunnel between the two wires and a charge-transfer mode appears.

I. INTRODUCTION

Plasmons are collective oscillatory modes of the electron system that are found in solids, at extended surfaces, and at the surface of confined metal structures[1]. The localized surface plasmon resonances sustained by metallic nanoparticles[2] have found widespread use in applications ranging from molecular spectroscopy[3] and chemical sensing[4], to photocatalysis[5] and photovoltaics[6]. Applications of plasmons in next generation nano-electronics[7] and quantum information technology[8] have also been envisioned. Advances in nano-fabrication techniques and transmission electron microscopy have recently enabled the study of plasmon excitations on a subnanometer length scale.[9] In particular, the use of

highly confined electron beams can provide spatial resolution of the electron energy loss spectrum (EELS) yielding unprecedented information about the dynamical properties of confined electron systems[10–13].

When the size of a plasmonic structure reaches the nano-scale, quantum effects begin to play a dominant role and the widely used classical models of electronic response become insufficient[14]. In this size regime, the theoretical description must be refined to account for quantum effects such as surface scattering, electron spill-out at the surface, coupling of plasmons to single-particle excitations, and the non-locality of the electronic response. We note that some of these effects, in particular the non-local response and spill-out, can be incorporated into semi-classical hydrodynamic models[1,15,16], however, the validity and predictive power of such an approach in the true quantum regime is not fully clarified.

One important hallmark of the quantum regime is electron tunneling which occurs when two systems are brought into close proximity. In fact tunneling leads to a breakdown of the local field enhancement predicted by the classical theory at sub-nanometer separations, and leads to the formation of a charge-transfer plasmon.[17–20]. Classically, the plasmon modes of a composite system can be obtained as even/odd combinations of the plasmon modes of the individual subsystems[21,22]. Recent experiments on coupled nanoparticles found the energy of hybridized modes to be blue-shifted relative to the classical result at separations less than 1 nm[23], and a semi-classical approach, using a quantum corrected model, found that the onset of quantum tunneling should occur at around 0.3 nm particle separation[24]. However, until now the influence of quantum effects on the spatial shape of the hybridized modes has not been explored.

In this work we apply a recently developed method[25] to compute and visualize the hybridization of the quantum plasmons of two parallel metallic nanowires at separations between 0 and 2 nm. The quantum plasmon modes are defined as certain eigenfunctions of the dynamical dielectric matrix, which we obtain using linear response TDDFT, and they represent the possible eigenmodes of the electron system damped by coupling to single-particle excitations.

We first show that the plasmon modes of single wires can be classified as surface or bulk modes with a specific angular symmetry index m and radial node index n. The maximum number of modes found for a given wire radius is limited by Landau damping which increases with n and m. For the double wire system, we find hybridized plasmon modes. For separations below 1.5 nm, the

hybrid modes begin to change in shape and their energy deviates from the classical result. These effects are caused by changes in the energy and wave function of electronic states lying several electron volts above the Fermi level (virtual tunneling). At separations below 2-3 Å we enter the true tunneling regime where the single-particle states around the Fermi energy start to overlap leading to an abrupt change in the energy and shape of the plasmon modes with certain modes disappearing and being replaced by a charge-transfer mode.

II.   METHOD

The DFT calculations have been carried out with the electronic structure code GPAW[26,27] using the Atomic Simulation Environment[28]. We study metallic Na wires with radii in the range 2 to 8 Å modeled within the jellium approximation. Here the ions are described with a constant positive background density that terminates abrupt at the edges, while the electron density is converged self-consistently. Since the jellium approach corresponds to a true free-electron metal, it is a good approximation to simple metals such as Na. The wire was constructed within a periodic supercell with 28 Å of vacuum perpendicular to the wire, see Fig. 1, showing the unit cell and the cal-culated densities within the jellium model. Electron spill-out extends approximately 3 Å outside the jellium edge, which is important for a correct description of surface plasmon modes in particular. The local density approximation (LDA) was used for exchange-correlation. The unit cell was sampled on grid-points of 0.2 Å spacing, and 20 k-points were used to map the 1D Brillouin zone along the wire, except for the study small momentum transfers in the response calculation where 80 k-points were used.

The microscopic dielectric function, $\epsilon_q(r, r', \omega)$, of the system was calculated using linear response TDDFT[29] within the random phase approximation (RPA), using a 15 eV energy cutoff for the reciprocal lattice vectors perpendicular to the wire and including electronic states 10 eV above the Fermi level. The dielectric function was sampled on an energy grid ranging from 0 to 10 eV with a spacing of 0.01 eV, and a broadening of 0.2 eV was applied to smear the discreteness in energy. The wave-vector along the wire, $q_\parallel$, was varied between 0.03 Å^{-1} and 0.8 Å^{-1} in order to study the energy dispersion. Convergence have been checked with respect to all parameters.

The plasmon eigenmodes were obtained by diagonalizing the dielectric function for each point on the frequency grid[25]. This leads to a set of distinct eigenvalue-curves
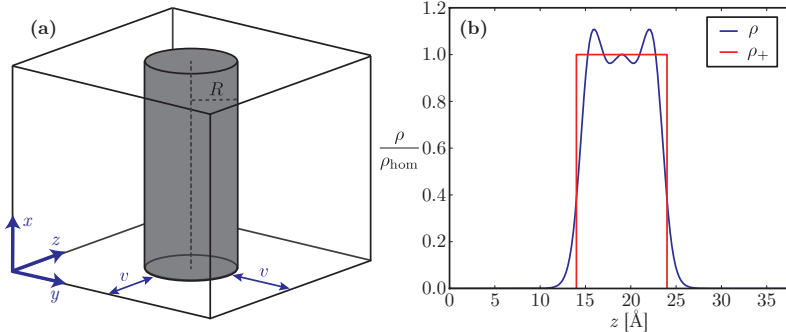
FIG. 1. (a) Sketch of the unit cell with gray region indicating the positive charge density of a cylindrical jellium wire, surrounded by vacuum $2v = 28$ Å. R is varied from 1 to 8 Å and the unit cell is 3 Å along the wire (b) Cross-sectional view of the wire showing the fixed positive background density profile ρ_+ (red) and the converged electron density ρ (blue), plotted relative to the free electron density of bulk Na, ρ_{hom}.

that evolves smoothly with frequency, each curve corresponding to a separate plasmon eigenmode, see Fig. 2. The corresponding eigenfunctions, $\phi_{\mathrm{ind}}(r, \omega_n)$, defines the spatial form of the induced potential (and density) of the eigenmodes. When the damping of the plasmon modes is small (which leads to a vanishing imaginary part of the eigenvalues), the eigenmodes can be identified at points where the real part crosses zero from negative to positive values. For larger damping, the maxima of the eigenvalue loss-spectrum, $-\mathrm{Im}\epsilon_q^{-1}(\omega, r, r')$, provide a more accurate measure of the energy of plasmon resonances. Since large damping is found in some cases, we have used the last approach throughout, and taken the half width of half maximum of the peaks as a measure of the plasmon energy. The real part of the

eigenvalue-curves each resembles a Drude-like behavior for the dielectric function, and has been fitted to a single-pole model:

$$\epsilon_n(\omega) = 1 - \frac{\alpha_n}{\omega - \beta_n + i\gamma_n}, \qquad (1)$$

which is used to find the mode strength, α_n. The parameter β_n corresponds to the average energy of the single particle transitions contributing the the given eigenmode, and γ_n is the damping of the mode.

III. RESULTS

The obtained plasmon eigenmodes for single wires of radius 2, 5 and 7.5 Å is shown in Fig. 3 (a)-(c), where the induced potential (first row) and density (second row) is plotted for increasing energy going left to right. The modes are characterized as sur-
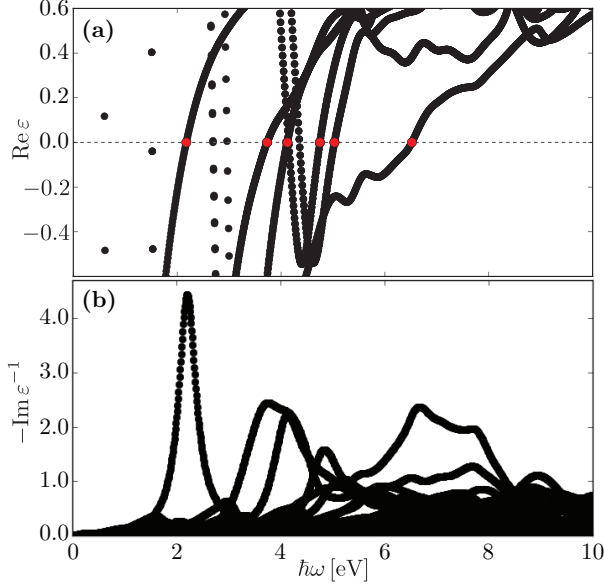
4

FIG. 2. (a) Real part of the eigenvalues of the dielectric function $\epsilon_q(\omega, r, r')$ for a 5 Å radius jellium wire. Each eigenvalue-curve that extends to negative values defines the existence of a plasmon eigenmode, and the crossing with zero from below (red points), approximates the plasmon energy of the current mode. (b) For a more correct description of the mode energies in the presence of large damping, maxima in the eigenvalues of $-\text{Im}\,\epsilon_q^{-1}(r, r', \omega)$ are used to define the plasmon frequencies, $\hbar\omega_n$.

face, S, or bulk, B, determined by the relative weight outside and inside the jellium perimeter, sketched in Fig. 3 (d). The potential and density of surface modes has a large contribution in the spill-out region outside the jellium edge, and has lower energy than the bulk modes. The modes are labeled according to their angular quantum number m, accounting for the $e^{im\theta}$ angular symmetry, easily visualized for the surface modes as the number of standing waves along the wire perimeter. For the thinnest wire only modes up to $m = 1$ are sustained, whereas modes with larger m are found for increasing radii. This corresponds to a minimum plasmon wavelength, $\lambda_{\text{min}} \approx 10$ Å that can exist for the structure, which is obtained by defining an effective wave-vector for the modes, $q_{\text{eff}}^2 = q_\parallel^2 + q_\perp^2$. The parallel momentum transfer $q_\parallel$ is fixed in the calculation, and $q_\perp$ can be written:

$$q_\perp = \frac{2\pi}{\lambda_\perp} = \frac{m}{R}, \tag{2}$$

where $\lambda_\perp$ is the wavelength associated with the shape of modes perpendicular to the wire. When m is sufficiently large, or R small, the effective wave-vector becomes large enough for the mode to enter the regime of Landau damping (coupling to intra-band transitions with large q), until the point where the mode can no longer be sustained. This is also reflected in a mode strength, α, that decreases with $m > 1$ for the surface modes.

For the bulk modes an additional quantum number, n, is required to account for radial dependence, where $B_{0,2}$ has an extra node in the induced density compared to $B_{0,1}$. From a group-theoretical analysis of the possible symmetries within the point-group $D_{\infty h}$, the modes with $m > 0$ are expected

(a) Radius 2 Å

	S_0	S_1^α	S_1^β
$\phi(\mathbf{r})$			
$\rho(\mathbf{r})$			
$\hbar\omega$	1.25 eV	3.61 eV	3.61 eV
α	0.75 eV	0.96 eV	0.96 eV

(b) Radius 5 Å

	S_0	S_1	S_2	S_3	$B_{1,1}$	$B_{0,1}$
$\phi(\mathbf{r})$		×2	×2	×2	×2	
$\rho(\mathbf{r})$						
$\hbar\omega$	2.21 eV	3.92 eV	4.13 eV	4.84 eV	6.65 eV	6.67 eV
α	1.93 eV	3.04 eV	1.51 eV	0.61 eV	0.71 eV	2.31 eV

(c) Radius 7.5 Å

	S_0	S_1	S_2	S_3	S_4	S_5	$B_{0,1}$	$B_{1,1}$	$B_{2,1}$	$B_{0,2}$
$\phi(\mathbf{r})$		×2	×2	×2	×2	×2			×2	×2
$\rho(\mathbf{r})$										
$\hbar\omega$	2.73 eV	3.85 eV	4.25 eV	4.43 eV	4.97 eV	5.73 eV	6.63 eV	7.07 eV	7.53 eV	7.80 eV
α	2.90 eV	3.44 eV	2.36 eV	1.42 eV	0.84 eV	0.62 eV	3.96 eV	2.97 eV	1.22 eV	0.60 eV

(d) Bulk and surface mode regions

bulk mode region

jellium perimeter   surface mode region

(e) Rotation symmetry and degeneracy

$\frac{2\pi}{m}$

$\frac{\pi}{2m}$

rotation symmetry angle

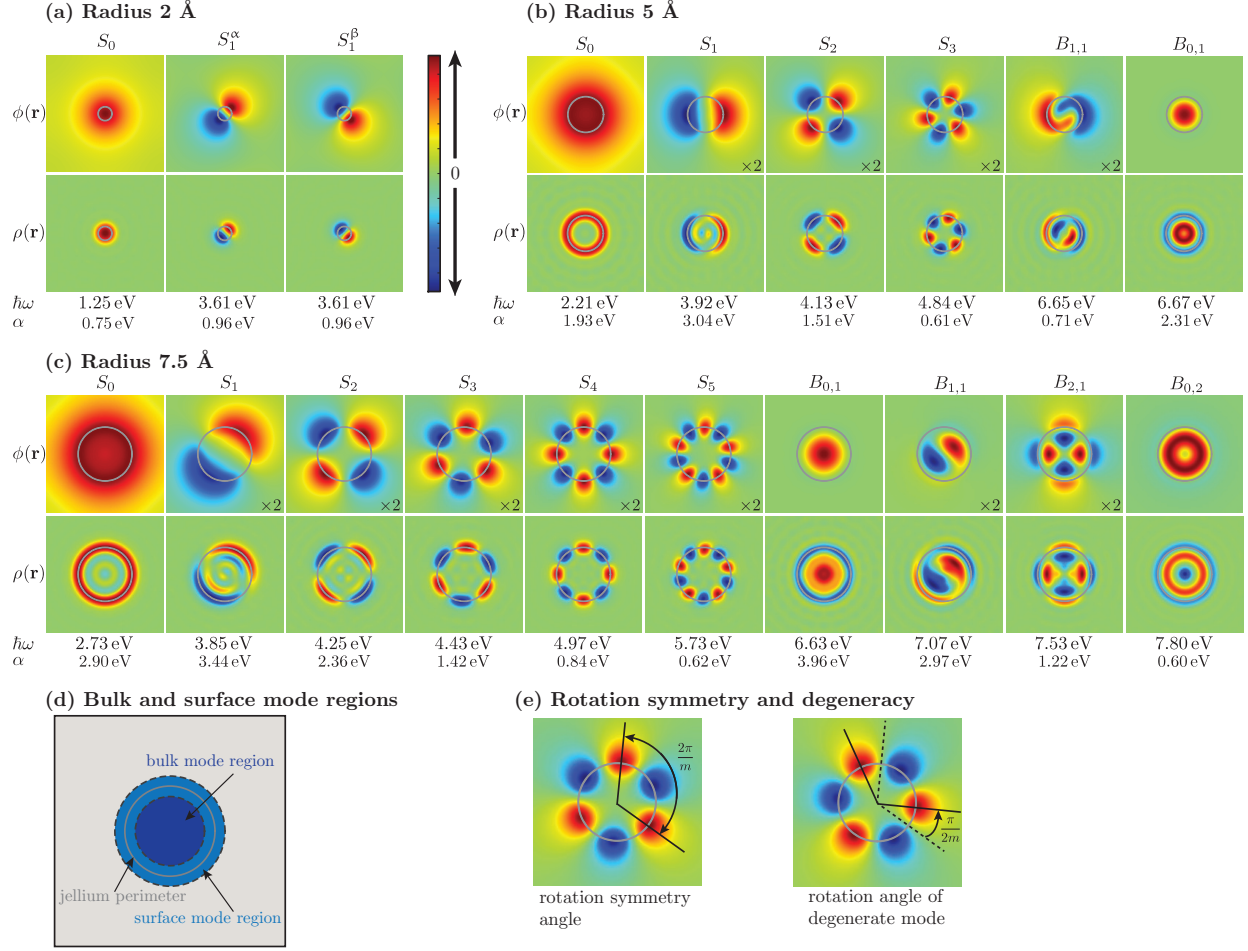rotation angle of degenerate mode

FIG. 3. Plasmon eigenmodes of Na jellium wires of radii: (a) 2 Å, (b) 5 Å, and (c) 7.5 Å, corresponding to induced potential, $\phi(\mathbf{r})$, and density, $\rho(\mathbf{r})$. The strength, α, and energy, $\hbar\omega$, is given for each mode. Modes with surface as well as bulk character are found, labelled S and B respectively, where the surface modes has a significant contribution in the spill-out region outside the jellium edge, see (d). The first subscript denotes the angular quantum number m, describing the $e^{im\theta}$ rotational symmetry. The increase in m leads to a larger effective wave-vector for the plasmon, q_{eff}, resulting in an increase in energy with m. Also the Landau damping increases with q_{eff}, which is why the a larger number of modes can be sustained by wires with larger radius. As explained in (e), modes with $m > 0$ appear as degenerate pairs, rotated with $\pi/2m$ (plots labeled ×2 when both are not shown).

to appear in degenerate pairs. This is exactly found for the calculated modes, where pairwise identical eigenvalue-curves results in identical modes with a relative rotation of $\pi/2m$, see Fig. 3 (e)

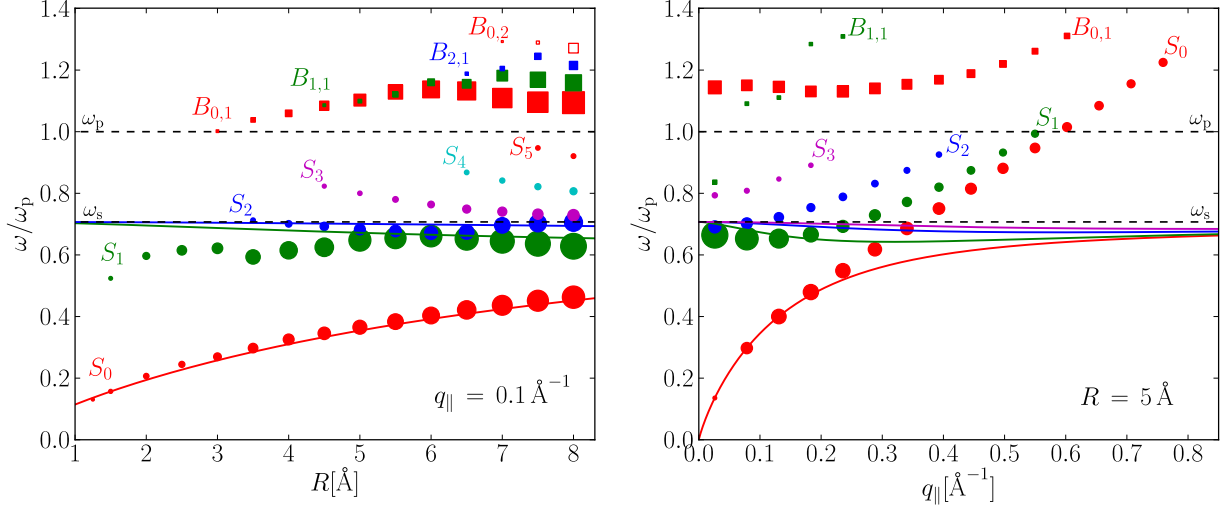We have investigated the energy disper-

FIG. 4. Energy dispersion of plasmon eigenmodes for the quantum calculations (circles and squares) and the classical results for the surface modes (solid lines). The energy is plotted against: (a) Wire radius for fixed $q_{\parallel} = 0.10\text{Å}^{-1}$. (b) Wave-vector $q_{\parallel}$ for fixed $R = 5\text{Å}$. Circles and squares represent surface and bulk modes respectively, and the diameter/height of the points indicate the mode strength, α, obtained by fitting the eigenvalues to a single pole model, Eq. 1. The S_0 mode, which has acoustic character, tends to zero energy for vanishing R or q, where there is a good agreement with the classical result. For large q the quantum model produces a positive dispersion for all modes, which is not captured by local models. For surface modes with $m > 0$, there is an overall poor agreement due to effects from a larger q_{eff} and spill-out.

sion of the modes with R and $q_{\parallel}$, shown in Fig. 4, where the result from our quantum calculation has been plotted together with the classical result obtained from solving Laplace's equation and using a local Drude model for the dielectric function[30]. The classical model yields a dispersion relation for the surface modes that depends on a single dimensionless parameter, qR, where q is the wave-vector parallel to the wire:

$$\omega_m^2 = \omega_p^2 \, qR \, I_m'(qR) \, K_m(qR). \quad (3)$$

Here I_m and K_m are the special Bessel's functions of order m, and ω_p is the bulk plasmon frequency. The acoustic character of the S_0 mode leads to an energy that goes to zero as a function of $q_{\parallel}R$, whereas the $S_{m>0}$ modes tends towards the classical surface plasmon frequency $\omega_P/\sqrt{2}$ for low $q_{\parallel}R$. For large $q_{\parallel}R$ all modes tends towards $\omega_P/\sqrt{2}$ for the classical result.

When comparing to our quantum results, a very good agreement is seen for the S_0

mode at low $q_\parallel$, which breaks down for larger $q_\parallel$. Since the Drude model assumes the electronic response to be local in space, it cannot capture the dispersion with q. This explains the significant deviation for large $q_\parallel$, where the quantum result for the energy continue to increase. This q-dependence also explains why the energy of the surface modes increases with larger m (due to a larger q_{eff}), opposed to the classical result where the energy does not exceed $\omega_P/\sqrt{2}$. However, S_1 and S_2, are seen to be red-shifted with respect to the classical value in the limit $q \to 0$, and for S_1 the redshift increases further with decreasing R. A redshift is expected for decreasing size of simple metal nanostructures due to electron spill-out; as the surface to bulk ratio increases, the spill-out will lead to a decrease in the mean electron density, which results in a lower plasmon frequency. This redshift was also observed for the plasmon eigenmodes of thin slabs of sodium[25], and for quantum calculation on small Na clusters[31]. This is opposed to the behavior of silver nanostructures, where coupling to single-particle transitions originating from the d-states of silver leads to blueshift with decreasing size[14,31]. Thus, there are two competing factors affecting the energy of the $S_{m>0}$ modes for decreasing R; the increase due to a larger perpendicular q, and the decrease due to spill out, which might explain the oscillatory behavior
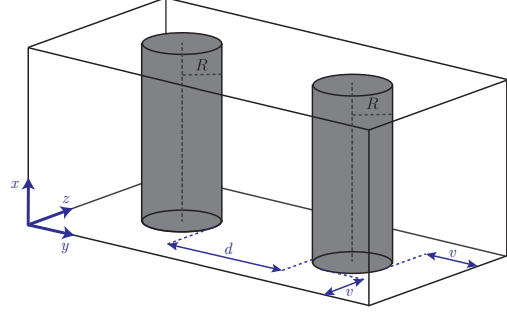

FIG. 5. The unit cell containing two jellium wires of distance d. We consider separations in the range 0 to 20 Å, and choose $R = 2.5$ Å for both wires, in order to study the case where only three modes exist for the individual wires.

of the S_1 mode for small R.

When considering the strength of the modes (represented by the diameter/height of the labels in Fig. 4), there is a clear tendency for weakening of modes for small R and large $q_\parallel$. This is due to a smaller number of electronic bands crossing the Fermi level for the thin wires, which gives a smaller number of transitions contributing to the plasmon in this limit. The weakening with increasing q can be explained by increasing Landau damping as discussed previously.

After establishing an understanding of the quantum modes of single wires, we are ready to study the hybridization of modes between two parallel wires of small separation. The unit cell is sketched in Fig. 5, where the separation, d, is varied from 20 Å down to zero measured from the jellium edge, and the

amount of vacuum separating the wires of neighboring super-cells are kept constant at 20 Å. The hybridization of plasmon modes is not unlike the formation of molecular orbitals as bonding and antibonding combinations of atomic orbitals[21,22], where the new hybridized modes correspond to the even and odd combinations of isolated modes of the individual structures. At very small separations however, this simplified description can no longer hold since overlap of the electronic states and eventual tunneling will alter the resonances. We have applied our quantum approach to provide real-space visualization of the hybridized modes in the transition from the non overlap to the overlap regime.

In order to limit the number of hybridized modes we choose both wire radii equal to 2.5 Å, where only the S_0 and the two degenerate S_1 modes exists. Only modes of similar symmetry will couple to form hybridized modes; for example, an S_0 mode at one wire will be unable of inducing a S_1-like potential at a neighboring wire, and no self-sustained oscillation can occur. Therefore the modes only couple to those of the same type (S_1 couple to the S_1 mode of same rotation), and six hybridized modes is predicted to exists for this structure.

Six modes are found in the quantum calculation as shown in Fig. 6(a), with eigenmodes calculated for a 20 Å separation of the wires.

In this regime of zero overlap between the electronic states, the modes can be classified according to conventional hybridization theory as even or odd combinations of the initial modes, labelled $++$ and $+-$ respectively, where the four S_1-types are further divided into vertical, v, and horizontal, h, according to the direction of polarization. As can be seen in Fig. 7 showing the induced potential and density for 8 Å, 2 Å, and 1 Å separations, this description is no longer valid for small separations.

The energy dispersion of the modes as a function of d is shown in Fig. 6(b), where the $+-$ and $++$ combinations split in energy for intermediate separations. A downshift is found for modes with opposite charges facing each other, i.e. S_0^{+-}, S_1^{h++}, and S_1^{v+-}, which can be explained by the electrostatic attraction between induced charges of opposite sign that leads to a lowering of the plasmon frequency (and in reverse for the other modes). The coupling between the wires increases for decreasing separations which leads to a larger splitting, until the tunneling regime is entered around 5 Å. The shift is more distinct for the S_0-types that also has the most long-ranged potential that explains the stronger coupling and larger splitting of bonding and antibonding modes. The potential from the electric dipole of the S_1 modes decreases faster along y, in particular for the vertical
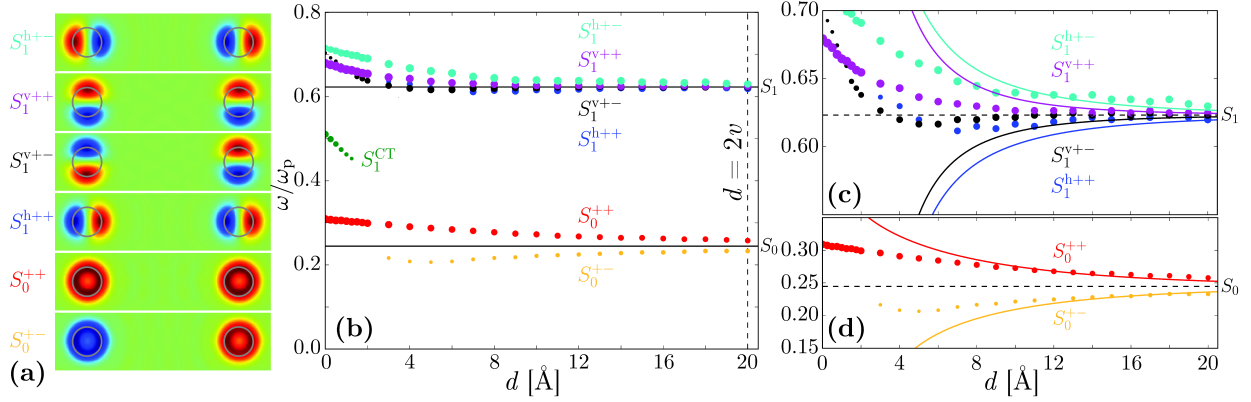
FIG. 6. (a) Induced density of hybridized modes of two parallel wires with $R = 2.5$ Å at 20 Å separation. The modes can be identified as hybridization between the S_0, S_1^α and S_1^β modes of the individual wires, where only modes of the same type couple due to symmetry restrictions. (b) The mode energies as a function of wire separation, d, with the mode strength indicated by the diameter of the points. The hybridization leads to a split in energy of the even, $++$, and odd, $+-$ mode-combinations, plotted together with the classical result (solid curves) in (c) and (d). At 2 Å separation the S_0^{+-} and $S_1^{\text{h}++}$ modes are quenched out due to tunneling and a charge-transfer mode S_1^{CT} appears.

modes, which again shows a smaller splitting than the horizontal modes.

In Fig. 6 (c) and (d) the quantum results have been plotted together with the results of a classical model. The later has been obtained by solving Laplace's equation for a system of two cylinders of equal radii R and dielectric constant $\epsilon = 1 - \frac{\omega_P^2}{\omega^2}$. Following a general approach by A. Moradi[32], we have derived the expressions for hybridized S_0 and S_1 modes for this system, see Appendix.

For separation > 15 Å there is a good agreement between the classical and quantum results for the energy splitting. For decreasing separations however, the quantum calculations produces a smaller splitting than the classical model, until all modes eventually shows a positive dispersion with decreasing d. For the S_0 modes the deviations from the classical model begins around $d = 10$ Å, whereas for the S_1 modes deviation is seen already at larger separation, approximately at $d = 15$ Å. We explain the deviation by a beginning overlap of unoccupied electronic states of the two wires that are more long-ranged, and thus provides a virtual electronic tunneling. At 10 Å separation, bands from 1.7 eV above the Fermi level were found to be modified compared to 20 Å separation, while noticeable changes in the
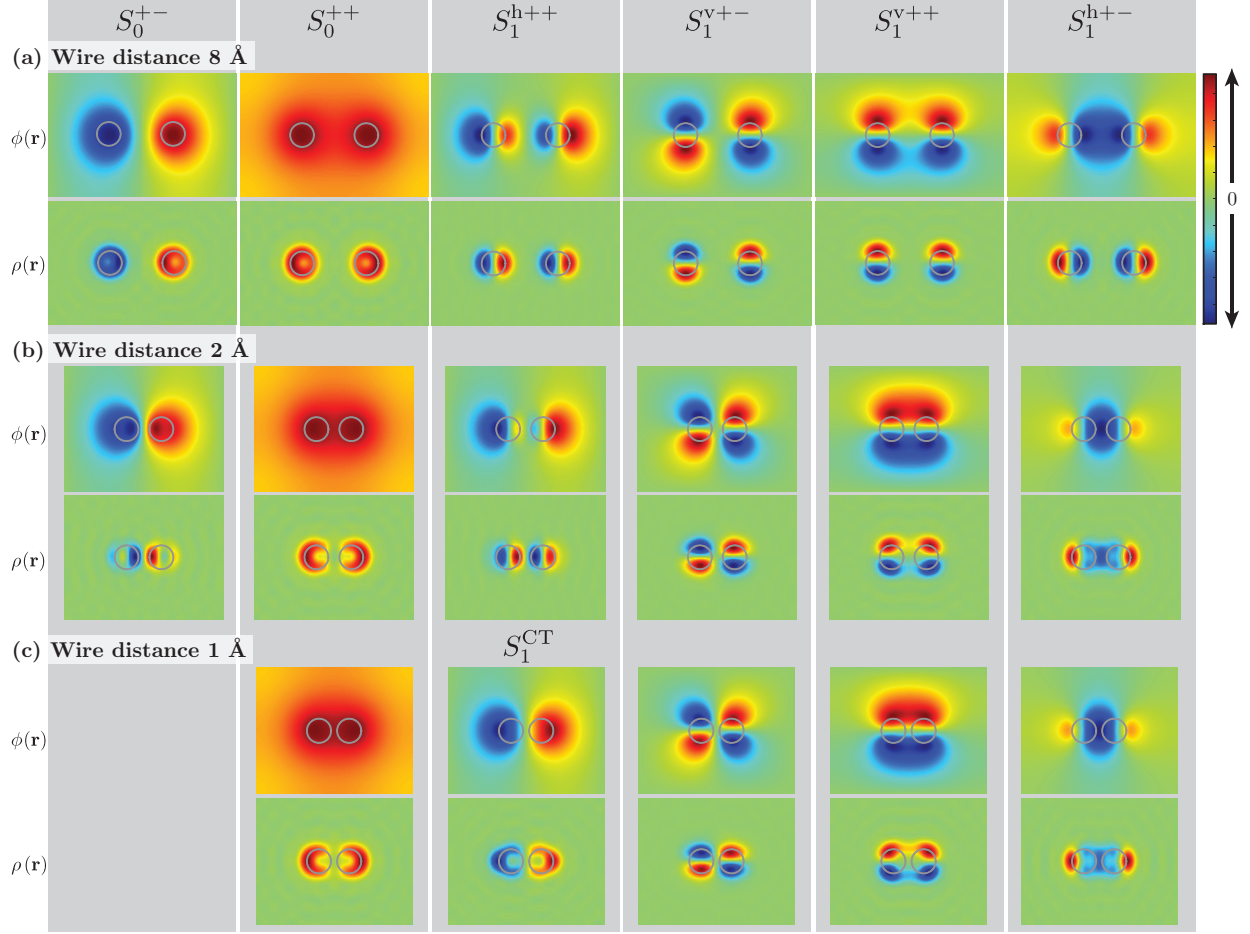
FIG. 7. The plasmon eigenmodes for two parallel nanowires with $R = 2.5$ Å for separations (a) 8 Å, (b) 2 Å and (c) 1 Å. Already at 8 Å separation the potential, $\phi(r)$, and density, $\rho(r)$, of the modes is slightly modified, the change being most dominant for the S_1^{h++} and S_0^{+-} modes. At 2 Å these mode are almost quenched out due to tunneling, and the induced density is shifted into the bulk. Below 2 Å a new charge-transfer mode S_1^{CT}, corresponding to density oscillation between the wires, appears. For the other modes there is a continuous evolution of shape from the non-touching to the touching regime, as seen for the mode energies as well.

occupied bands were only found below 4 Å separation.

Our approach for visualizing the eigenmodes from a quantum calculation provides a clear picture of how the plasmon modes are altered due to these quantum effects. As can be seen in Fig. 7, already at 8 Å separation some eigenmodes are modified compared to the large separation limit shown in Fig. 6 (a). The modes are seen to be gradually altered with decreasing separation, with the S_0^{+-} and S_1^{h++} modes being most seri-

11

ously affected due to the facing of opposite charges. The potential between the wires decreases in amplitude going from 8 Å to 2 Å separation, and the induced density is shifted further into the bulk. A decrease in mode strength (indicated by the marker diameter in Fig. 6) is also found for these modes upon approaching 2 Å separation. At 1 Å both modes are quenched due to tunneling and are replaced by a dipolar charge-transfer mode, here named S_1^{CT}, and the induced density is now located at the other side of the wires, away from the interface. That this mode is different in nature than the S_1^{h++} and S_0^{+-} is also clear from Fig. 6(b), where it appears as a separate line in the energy dispersion just below 2 Å, and increases in strength for smaller separations. In this touching regime with large degree of tunneling, the structure can be regarded as one (non-cylindrical) wire; however, for the other modes there is a continuous transition from the non-touching to the touching regime. The S_1^{V++} and S_1^{h+-} modes gradually build up induced density in the region between the wires, and S_1^{V+-} ends up resembling a quadropolar ($m=2$) mode for the joint structure.

IV. CONCLUSION

We have given a visual demonstration of the plasmon eigenmodes in nano-wires and

shown how the hybridized plasmon modes of a two-wire system is modified due to quantum effects for decreasing separation. For separations above 15 Å the modes were well characterized according to conventional hybridization theory, and a good correspondence was found with a classical model for the splitting of even and odd modes. This agreement was found to break down starting from 10 Å to 15 Å separation, where our quantum calculations produced a significant smaller splitting. We attribute this to virtual electronic tunneling due to overlap between unoccupied states, which in the range of 5-15 Å separation is strong enough to decrease the induced density (and potential) in the interface, which results in a lower energy splitting. Below 5 Å the dispersion shows a qualitatively different behavior with an increase in energy for all modes, indicating an larger degree of tunneling. However; only for separations below 2 Å did we find a true charge-transfer plasmon to appear.

Appendix: Classical hybridization model for a two-wire system

We have derived the classical expression for the energy of the hybridized modes of a system of two cylinders of equal radii R, where the general approach by A. Moradi[32] simplifies to finding the zeros of the deter-

minant of the matrix: $(\mathbf{M}^2 - I)$, where the elements of $\mathbf{M}$ are written:

$$M_{mn} = \frac{\omega_m^2}{\omega^2 - \omega_m^2} \frac{K_{m+n}(qd)I_m(qR)}{K_n(qR)}, \quad \text{(A.1)}$$

where the m, n indices corresponds to angular quantum numbers, and ω_m is the energy of the S_m mode of a single wire given in Eq. 3. For the coupling of two S_0 modes both $m, n = 0$, and solving for omega yields two solutions:

$$\omega_\pm^2 = \omega_0^2\Big[1 \pm K_0(qd)\frac{I_0(qR)}{K_0(qR)}\Big], \qquad \text{(A.2)}$$

accounting for the splitting of the S_0^{+-} and S_0^{++} modes. Due to the small discrepancy between the quantum results and the classical model for a single wire (due to dispersion with q and R), we have set ω_0 equal to the result from the quantum calculation for S_0 for a clearer comparison. For coupling of S_1 modes, $m, n = \pm 1$, and $(\mathbf{M}^2 - I)$ is a 2 by 2 matrix, which leads to a total of four solutions for ω:

$$\omega_{\{h,v\},\{\pm\}}^2 = \omega_1^2\Big[1\{\pm,\mp\}\frac{I_1(qR)}{K_1(qR)}\sqrt{K_2(qd)^2 + K_0(qd)^2 \pm 2K_0(qd)K_2(qd)}\,\Big], \qquad \text{(A.3)}$$

where ω_1 has been set equal to the quantum result for S_1.

ACKNOWLEDGMENTS

* kiran@fysik.dtu.dk

[1] J. M. Pitarke, V. M. Silkin, E. V. Chulkov, and P. M. Echenique, Reports on Progress in Physics **70**, 1 (2007).

[2] K. Willets and R. Van Duyne, Annu. Rev. Phys. Chem. **58**, 267 (2007).

[3] K. Kneipp, Y. Wang, H. Kneipp, L. Perelman, I. Itzkan, R. Dasari, and M. Feld, Physical Review Letters **78**, 1667 (1997).

[4] E. Larsson, C. Langhammer, I. Zorić, and B. Kasemo, Science **326**, 1091 (2009).

[5] T. Hirakawa and P. Kamat, Journal of the American Chemical Society **127**, 3928 (2005).

[6] H. Atwater and A. Polman, Nature materials **9**, 205 (2010).

[7] K. F. MacDonald, Z. L. Sámson, M. I. Stockman, and N. I. Zheludev, Nature Photonics

3, 55 (2008).

[8] A. Huck, S. Kumar, A. Shakoor, and U. L. Andersen, Physical review letters **106**, 96801 (2011).

[9] F. J. García de Abajo, Reviews of modern physics **82**, 209 (2010).

[10] M. Bosman, V. J. Keast, M. Watanabe, A. I. Maaroof, and M. B. Cortie, Nanotechnology **18**, 165505 (2007).

[11] A. L. Koh, K. Bao, I. Khan, W. E. Smith, G. Kothleitner, P. Nordlander, S. A. Maier, and D. W. McComb, ACS nano **3**, 3015 (2009).

[12] B. S. Guiton, V. Iberi, S. Li, D. N. Leonard, C. M. Parish, P. G. Kotula, M. Varela, G. C. Schatz, S. J. Pennycook, and J. P. Camden, Nano letters **11**, 3482 (2011).

[13] I. Alber, W. Sigle, F. Demming-Janssen, R. Neumann, C. Trautmann, P. A. van Aken, and M. E. Toimil-Molares, ACS nano **6**, 9711 (2012).

[14] J. A. Scholl, A. L. Koh, and J. A. Dionne, Nature **483**, 421 (2012).

[15] S. Raza, G. Toscano, A.-P. Jauho, M. Wubs, and N. A. Mortensen, Phys. Rev. B **84**, 121412 (2011).

[16] C. David and F. J. García de Abajo, The Journal of Physical Chemistry C **115**, 19470 (2011).

[17] I. Romero, J. Aizpurua, G. W. Bryant, and F. J. García de Abajo, Opt. Express **14**, 9988 (2006).

[18] J. Lassiter, J. Aizpurua, L. Hernandez, D. Brandl, I. Romero, S. Lal, J. Hafner, P. Nordlander, and N. Halas, Nano letters **8**, 1212 (2008).

[19] J. Zuloaga, E. Prodan, and P. Nordlander, Nano Letters **9**, 887 (2009), pMID: 19159319.

[20] R. Esteban, A. G. Borisov, P. Nordlander, and J. Aizpurua, Nature Communications **3**, 825+ (2012).

[21] E. Prodan, C. Radloff, N. J. Halas, and P. Nordlander, **302**, 419 (2003).

[22] H. Wang, D. W. Brandl, P. Nordlander, and N. J. Halas, Accounts of Chemical Research **40**, 53 (2007), pMID: 17226945.

[23] J. Kern, S. Großmann, N. V. Tarakina, T. Häckel, M. Emmerling, M. Kamp, J.-S. Huang, P. Biagioni, J. C. Prangsma, and B. Hecht, Nano Letters **12**, 5504 (2012).

[24] K. J. Savage, M. M. Hawkeye, R. Esteban, A. G. Borisov, J. Aizpurua, and J. J. Baumberg, Nature **491**, 574 (2012).

[25] K. Andersen, K. W. Jacobsen, and K. S. Thygesen, Phys. Rev. B **86**, 245129 (2012).

[26] J. J. Mortensen, L. B. Hansen, and K. W. Jacobsen, Phys. Rev. B **71**, 035109 (2005).

[27] J. Enkovaara, C. Rostgaard, J. Mortensen, J. Chen, M. Dulak, L. Ferrighi, J. Gavnholt, C. Glinsvad, V. Haikola, H. Hansen, H. Kristoffersen, M. Kuisma, A. Larsen, L. Lehtovaara, M. Ljungberg, O. Lopez-

Acevedo, P. Moses, J. Ojanen, T. Olsen, V. Petzold, N. Romero, J. Stausholm-Moller, M. Strange, G. Tritsaris, M. Vanin, M. Walter, B. Hammer, H. Hakkinen, G. Madsen, R. Nieminen, J. Nrskov, M. Puska, T. Rantala, J. Schiotz, K. Thygesen, and K. Jacobsen, Journal of Physics: Condensed Matter **22** (2010).

[28] S. Bahn and K. Jacobsen, Computing in Science Engineering **4**, 56 (2002).

[29] J. Yan, J. J. Mortensen, K. W. Jacobsen, and K. S. Thygesen, Phys. Rev. B **83**, 245122 (2011).

[30] J. L. Gervasoni and N. R. Arista, Phys. Rev. B **68**, 235302 (2003).

[31] A. Liebsch, Phys. Rev. B **48**, 11317 (1993).

[32] A. Moradi, Physics of Plasmas **18**, 064508 (2011).